Stability and superconductivity of lanthanum and yttrium decahydrides

Alice M. Shipley,[*] Michael J. Hutcheon,[†] Mark S. Johnson, and Richard J. Needs

Theory of Condensed Matter Group, Cavendish Laboratory,
J. J. Thomson Avenue, Cambridge CB3 0HE, United Kingdom

Chris J. Pickard

Department of Materials Science and Metallurgy,
27 Charles Babbage Rd, Cambridge CB3 0FS, United Kingdom and
Advanced Institute for Materials Research, Tohoku University,
2-1-1 Katahira, Aoba, Sendai, 980-8577, Japan

Rare-earth hydrides can exhibit high-temperature superconductivity under high pressure. Here, we apply a crystal structure prediction method to the current record-holding T_c material, LaH_{10}. We find a pressure-induced phase transition from the experimentally observed cubic phase to a hexagonal phase at around 420 GPa. This new phase is metastable down to low pressures and could explain experimental observations of hcp impurities in fcc samples. We go on to find that YH_{10} adopts similar structures and discuss the sensitivity of superconductivity calculations to certain computational parameters.

I.   INTRODUCTION

Hydrogen was predicted to be a room-temperature superconductor at very high pressure in 1968 [1], but the pressures required to metallise hydrogen are difficult to obtain [2–7]. Hydrides have been suggested to have lower metallisation pressures than pure hydrogen due to *chemical pre-compression* [8] and therefore might become superconducting at more readily accessible pressures. This idea has motivated a surge of research examining potential superconductivity in high-pressure hydrides, with several reviews summarising recent developments [9–15].

Theoretical studies of ScH_3, LaH_3 [16], YH_3, YH_4 and YH_6 [17–19] identified hydrides of rare-earth elements as potential high-temperature superconductors. First-principles structure searching studies of rare-earth hydrides have reported structures with high hydrogen content adopting cage-like structures [20, 21]. Of particular note, a T_c of 264-286 K was calculated for $Fm\bar{3}m$ LaH_{10} at 210 GPa [20], while the analogous YH_{10} structure was calculated to have $T_c = 305$-326 K at 250 GPa. Slight distortions of the cubic LaH_{10} phase were found to lead to $C2/m$ and $R\bar{3}m$ structures at lower pressures [22, 23], though Ref. [24] showed that quantum effects render $Fm\bar{3}m$ as the true ground state. These predictions were followed by experimental measurement of critical temperatures reaching 260 K in LaH_{10} at 170-200 GPa [25, 26]. The high-T_c phase was determined to be a structure with an fcc arrangement of La atoms, lending support to theoretical predictions.

In addition to the aforementioned studies, others have focused on heavier rare-earth hydrides, exploring the synthesis and superconducting properties of cerium [27, 28], praseodymium [29] and neodymium [30] hydrides. Here,

within the framework of density functional theory (DFT) [31, 32], we revisit LaH_{10} and YH_{10} using crystal structure prediction methods. We find a phase transition to a new hexagonal phase in LaH_{10} at high pressures, with the metastability of this phase at low pressures offering an explanation for the experimental observation of hcp impurities in fcc samples [26]. We go on to predict the phases and corresponding critical temperatures that may be observed in YH_{10}.

II.   THEORY AND METHODOLOGY

A.   Phonons and superconductivity

The Hamiltonian of a coupled electron-phonon system [33] can be written as

$$
H = \underbrace{\sum_{kn} \epsilon_{nk} c_{nk}^{\dagger} c_{nk}}_{\text{electronic dispersion}} + \underbrace{\sum_{q\nu} \omega_{q\nu}\left(a_{q\nu}^{\dagger} a_{q\nu} + \frac{1}{2}\right)}_{\text{phonon dispersion}} +
$$
$$
\underbrace{\frac{1}{\sqrt{N_p}} \sum_{kqmn\nu} g_{mn\nu}(k,q) c_{m,k+q}^{\dagger} c_{nk}\left(a_{q\nu} + a_{-q\nu}^{\dagger}\right)}_{\text{electron-phonon coupling}}. \tag{1}
$$

In this work, we calculate the electronic Kohn-Sham eigenvalues ϵ_{nk}, phonon frequencies $\omega_{q,\nu}$, and electron-phonon coupling constants $g_{mn\nu}(k,q)$ appearing in H from first-principles using the QUANTUM ESPRESSO DFT code [34, 35], which we optimised for this work [36]. The Hamiltonian in Eq. 1 can be treated within Migdal-Eliashberg theory [37], allowing us to define the electron-boson spectral function

$$
\alpha^2 F(\omega) = \frac{1}{N(\epsilon_F)} \sum_{mnq\nu} \delta(\omega - \omega_{q\nu}) \sum_k |g_{mn\nu}(k,q)|^2
$$
$$
\times \delta(\epsilon_{m,k+q} - \epsilon_F)\delta(\epsilon_{n,k} - \epsilon_F). \tag{2}
$$

* ams277@cam.ac.uk
† mjh261@cam.ac.uk

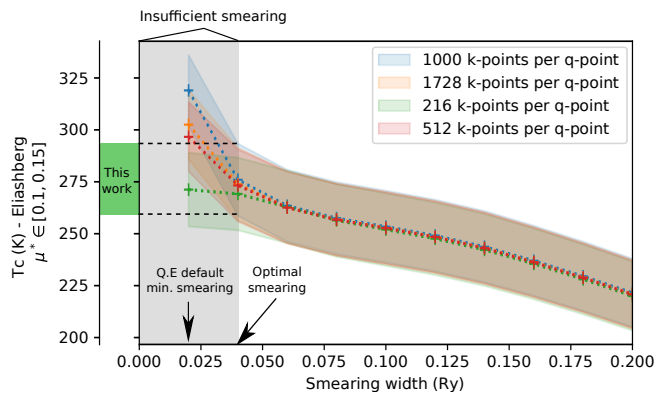FIG. 1. The dependence of T_c on the double-delta smearing width, σ, for $Fm\bar{3}m$-YH$_{10}$ at 350 GPa. The region of insufficient smearing is shown, along with our choice of σ for this structure and pressure. The smallest value used in an electron-phonon calculation with default QUANTUM ESPRESSO settings is shown.

FIG. 2. The dependence of T_c on the double-delta smearing width, σ, for $Im\bar{3}m$-YH$_6$ at 160 GPa. A recent experimental measurement at 166 GPa, falling just within our calculated T_c range, is also shown [43]. We note that Refs. [43, 44] highlighted that previous calculated T_c values were considerably higher than their experimental observations and that the results of Ref. [19], which used accurate Wannier interpolation techniques, are in agreement with ours.

From $\alpha^2 F$ we extract the superconducting critical temperature by solution of the Eliashberg equations using the ELK code [38]. From the quantities appearing in H we may also construct the electronic and vibrational densities of states, from which we can derive the Gibbs free energy as a function of temperature. We do this at a range of pressures, allowing us to construct pressure-temperature phase diagrams.

To evaluate the double-delta sum in Eq. 2 for finite $\mathbf{k}$- and $\mathbf{q}$-point grids, we follow the method detailed in Appendix A of Ref. [39] and smear the delta functions with finite-width Gaussians. In order to best approximate the delta functions, the smallest sensible smearing should be used. However, the smearing must be large enough to accommodate the finite $\mathbf{k}$-point grids used. We identify the optimal choice of smearing from discrepancies in the results between different $\mathbf{k}$-point grids [39], as can be seen in Figs. 1 and 2.

Our electron-phonon calculations were carried out using the Perdew-Burke-Ernzerhof (PBE) generalised gradient approximation [40] and ultrasoft pseudopotentials, validated against the all-electron WIEN2k code [41, 42]. Well-converged $\mathbf{k}$-point grids with a spacing of at most $2\pi \times 0.015$ Å^{-1} and an 820 eV plane wave cut-off were used [42]. The $\mathbf{q}$-point grids used were typically 8 times smaller than the $\mathbf{k}$-point grids and were Fourier interpolated to 10 times their original size. For the cubic systems studied, this corresponds to $\geq 24 \times 24 \times 24$ $\mathbf{k}$-point grids and a $3 \times 3 \times 3$ $\mathbf{q}$-point grid Fourier-interpolated to $30 \times 30 \times 30$.

B. Structure searching

Our structure searching calculations were performed using *ab initio* random structure searching (AIRSS) [14, 45] and CASTEP [46]. The PBE functional, CASTEP QC5
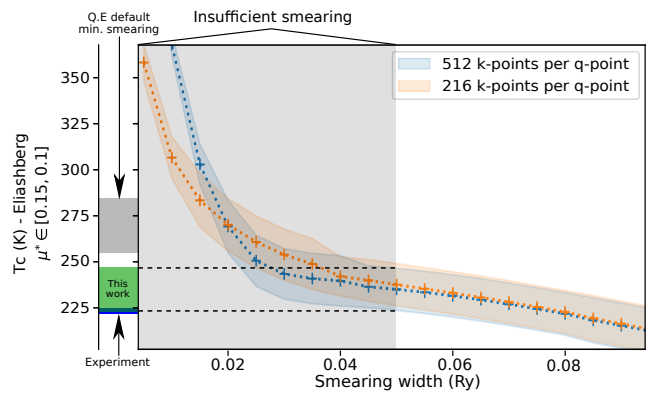
pseudopotentials, a 400 eV plane wave cut-off and a $\mathbf{k}$-point spacing of $2\pi \times 0.05$ Å^{-1} were used in these searches unless otherwise stated. The C2X software [47] was used for converting between CASTEP and QUANTUM ESPRESSO file formats, and also for reporting the space groups of structures at various tolerances.

III. RESULTS AND DISCUSSION

In the following sections, we report results in terms of phonon-corrected pressures, obtained by fitting the Birch-Murnaghan equation of state [48] to our data. Where static DFT pressures are reported instead, they are labelled as P_{DFT} - this second set of pressures facilitates comparison with previous calculations as they are simply an input parameter to the DFT geometry optimisation.

A. LaH$_{10}$

Low enthalpy candidates found by AIRSS for LaH$_{10}$ include the space groups $Fm\bar{3}m$, $R\bar{3}m$, and a 2-formula-unit $C2/m$, which had been identified previously. The searches also revealed a new structure of $P6_3/mmc$ symmetry. These structures are shown in Fig. 3. A $C2/m$ structure with 3 formula units per unit cell was also found to be energetically competitive, but was not considered further in this work as it behaves similarly to the 2-formula unit phase over the pressure range of interest. We also found several previously unreported structures at low pressures with space groups $Pnnm$, $C2$ and $P2_12_12_1$ and unit cells containing 2, 3 and 4 formula units, respectively. These are the lowest enthalpy structures in
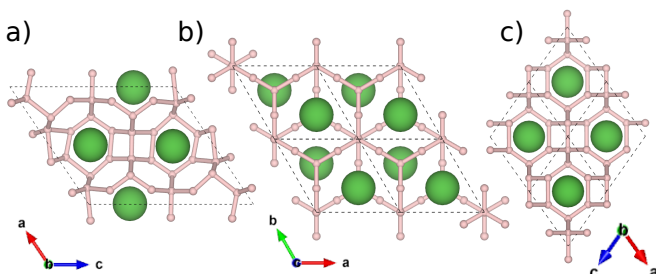
FIG. 3. Structures of LaH$_{10}$. (a) 2 formula unit/cell $C2/m$, (b) 2 formula unit/cell $P6_3/mmc$, (c) 1 formula unit/cell $Fm\bar{3}m$. The $R\bar{3}m$ structure is not shown as it is visually indistinguishable from the $Fm\bar{3}m$ structure at the pressures of interest.
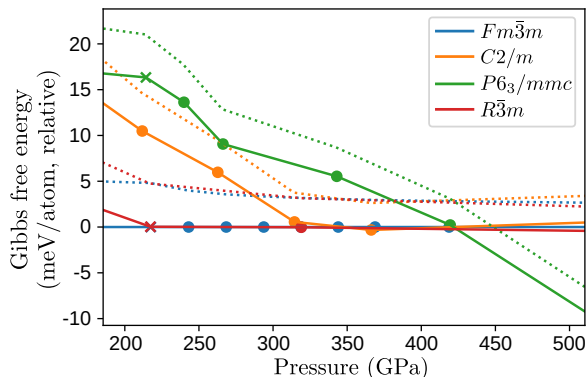

FIG. 4. The Gibbs free energy as a function of pressure for energetically competitive phases of LaH$_{10}$, plotted relative to a third-order Birch-Murnaghan fit of the $Fm\bar{3}m$ data. Crosses represent calculations with unstable phonon modes - these points are not included in the Gibbs free energy fit. Solid lines are at 300 K, dashed lines are at 0 K.
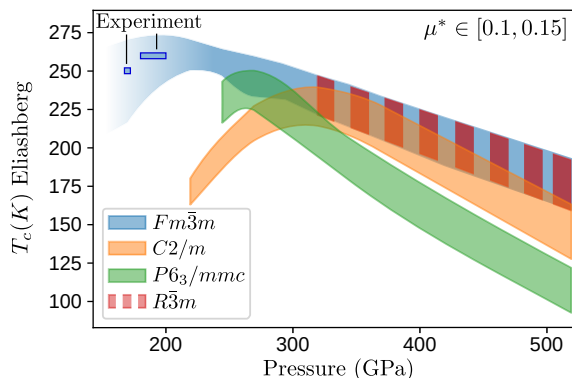

FIG. 5. Calculated $T_c(P)$ for dynamically stable phases of LaH$_{10}$ from direct solution of the Eliashberg equations. The width of the lines arises from our treatment of the Morel-Anderson pseudopotential, μ^*, [49] as an empirical parameter with values between 0.1 and 0.15. The $Fm\bar{3}m$ result has been extended into the region where it is dynamically unstable (shaded according to unstable fraction of the phonon density of states) in order to facilitate comparison with the experimental results of Refs. [25, 26]. This extension was achieved by removing the contribution of unstable phonon modes, in their entirety, to the Eliashberg function while maintaining its normalisation.
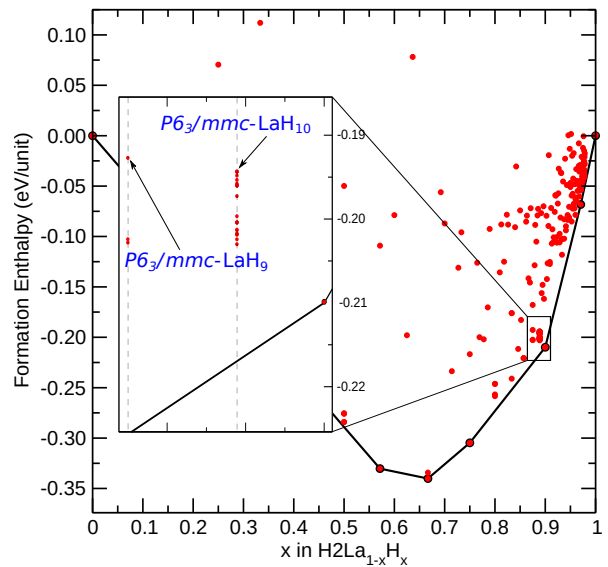

FIG. 6. A convex hull for the La-H system at 150 GPa, accurately calculated using CASTEP, $\mathbf{k}$-point spacing of $2\pi\times0.03$ Å^{-1} and a 700 eV plane-wave cut-off. The on-the-fly pseudopotential strings used are provided in the supplementary material [42]; the inclusion of a fraction of a 4f electron in the generation of the La pseudopotential was found to be crucial. A pseudopotential without this addition was unable to reproduce the all-electron $Fm\bar{3}m$-LaH$_{10}$ PV curve and led to a qualitatively different convex hull [42]. In agreement with Ref. [50], we find that LaH$_9$ is not on the hull at this pressure. However, we also find that LaH$_{16}$ does not lie on the hull at 150 GPa, despite finding the $P6/mmm$-LaH$_{16}$ structure studied in that work.

the low pressure region [42]. However, we note that these structures are distortions of the high-symmetry $Fm\bar{3}m$ structure and, similarly to the case of $R\bar{3}m$ noted in Ref. [24], it is possible that anharmonic effects may remove them from the potential energy surface. In addition to this, the low symmetry and large unit cells of these structures make converged phonon calculations prohibitively expensive; they are therefore not considered further in this work.

The calculated LaH$_{10}$ phase behaviour is shown in Fig. 4 and the corresponding critical temperatures are shown in Fig. 5. Our calculations for the $Fm\bar{3}m$ phase include unstable phonon modes for $P_{DFT} \leq 210$ GPa. In the harmonic picture, explicitly taking into account this dynamical instability leads to a window of stability for the $C2/m$ phase [42], which is in agreement with previous calculations [22, 23]. However, we note that under the assumption that the unstable modes can be neglected in the calculation of the Gibbs free energy, we obtain the same behaviour as the anharmonic calculations of Ref. [24], i.e., $Fm\bar{3}m$ is the only phase with a predicted region of stability at lower pressures. With increasing pressure, as noted in previous theoretical work [24], the $R\bar{3}m$ structure approaches $Fm\bar{3}m$ symmetry. We therefore expect that these phases will not be distinguishable at high

pressures.

At 300 K, the $P6_3/mmc$ structure becomes thermodynamically favourable at pressures above ~420 GPa. More importantly, this hexagonal phase is also metastable at low pressures, lying within 20 meV/atom of the cubic phase down to 150 GPa, and therefore provides an explanation for the experimental observation of hcp impurities in fcc-LaH_{10} samples at 170 GPa in Ref. [26].

A low-energy hexagonal LaH_9 structure predicted previously in similar pressure regions [50] could offer an alternative explanation for the observation of these impurities. However, the authors of Ref. [26] determined that the two kinds of hcp impurities in their fcc-LaH_{10} samples possessed LaH_{10} stoichiometry. We also calculated a high-quality La-H convex hull at 150 GPa using AIRSS [45] and qhull [51] (see Fig. 6). It shows that the $P6_3/mmc$-LaH_{10} structure predicted in this work lies closer to the hull than the $P6_3/mmc$-LaH_9 structure of Ref. [50]. It is therefore likely that the hcp impurities originate from our new $P6_3/mmc$-LaH_{10} phase.

To facilitate comparison with experiment, we have calculated powder X-ray diffraction patterns for cubic and hexagonal LaH_{10} and hexagonal LaH_9 at 150 GPa - we supply these, alongside the calculated c/a ratios and volumes in the supplementary material [42].

We calculate $T_c = 232$-259 K for $Fm\bar{3}m$-LaH_{10} at 269 GPa ($P_{DFT}=250$ GPa), which is lower than the previous theoretical result of $T_c = 257$-274 K [20]. However, we observe an increase in T_c on reduction of the double-delta smearing parameter to below our calculated optimal value [42], potentially explaining this discrepancy. Careful choice of smearing has previously been noted as important in other hydride systems [52]. We also note a previous calculation of T_c for this structure at 200 GPa [21], however, in agreement with other calculations [22, 23] we find $Fm\bar{3}m$ to be dynamically unstable at this pressure. This dynamical instability means we cannot directly compare with experiment, which found T_c = 250 K at around 170 GPa [26] and T_c = 260 K at 180-200 GPa [25]. However, ignoring the contribution of the unstable phonon modes to the Eliashberg function at pressures ≤ 210 GPa allows for a rough estimation of T_c in these regions; this is depicted as the faded-out section in Fig. 5 and the results obtained are in agreement with experimental results. For the $C2/m$ phase, using an optimal value of smearing we calculate $T_c = 205$-225 K at 262 GPa ($P_{DFT}=250$ GPa), compared to $T_c = 229$-245 K in Ref. [23].

B. YH_{10}

Low-enthalpy candidates for YH_{10} found using AIRSS include $Fm\bar{3}m$, which had been identified previously, a slight distortion of this phase, $R\bar{3}m$, and structures of $P6_3/mmc$ and $Cmcm$ symmetry. These structures are shown in Fig. 7. The calculated YH_{10} phase behaviour is shown in Fig. 8 and the corresponding critical tem-
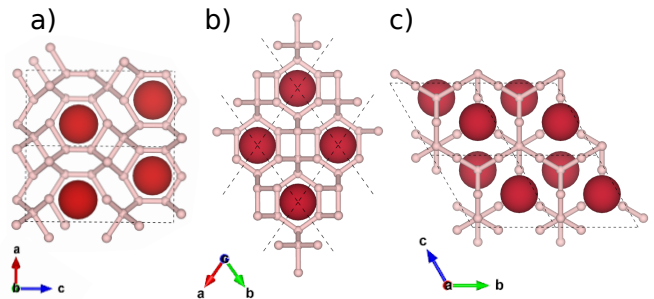

FIG. 7. Structures of YH_{10}. (a) 2 formula unit/cell $Cmcm$, (b) 1 formula unit/cell $Fm\bar{3}m$, (c) 2 formula unit/cell $P6_3/mmc$. The $R\bar{3}m$ structure is, again, not shown.
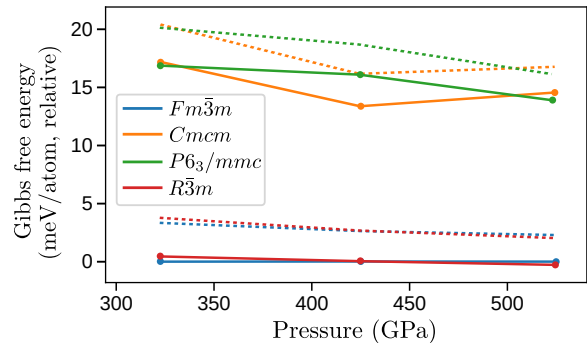

FIG. 8. The Gibbs free energy as a function of pressure for energetically competitive phases of YH_{10}, plotted and interpolated relative to a third-order Birch-Murnaghan fit of the $Fm\bar{3}m$ data. Solid lines are at 300 K, dashed lines are at 0 K.
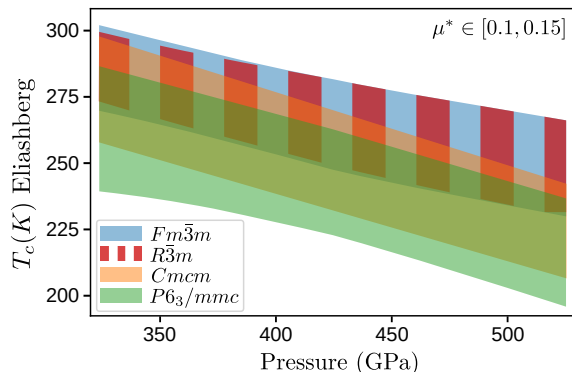

FIG. 9. Calculated $T_c(P)$ for dynamically stable phases of YH_{10} from direct solution of the Eliashberg equations. μ^* is, again, taken to have a value between 0.1 and 0.15.

peratures are shown in Fig. 9. We do not predict any phase transitions within the predicted range of stability of the YH_{10} stoichiometry [21]. However, the difference in Gibbs free energy between the $Fm\bar{3}m$ and $R\bar{3}m$ phases is exceedingly small (see Fig. 8), reflecting their structural similarity.

Previous calculations for $Fm\bar{3}m$ found $T_c = 305$-326 K

at 250 GPa [20] and $T_c = 303$ K at 400 GPa [21]. Here, we calculate $T_c = 270\text{-}302$ K at 324 GPa (P_{DFT}=300 GPa) and $T_c = 250\text{-}280$ K at 425 GPa (P_{DFT}=400 GPa). Our more conservative T_c results can again be explained by considering the smearing parameter used to approximate the double-delta integral in Eq. 2. We were able to reproduce the results of previous calculations by using the minimum default smearing employed in QUANTUM ESPRESSO, which in this case overestimates T_c by ∼30 K (see Fig. 1) compared to optimal smearing. We note that our results agree with those obtained using Wannier interpolation techniques [19]. Using the same method to calculate an optimal smearing also provides results in agreement with recent experimental measurements for $Im\bar{3}m$-YH$_6$ [43], as shown in Fig. 2.

IV. CONCLUSIONS

We have identified a new hexagonal phase of LaH$_{10}$ with $P6_3/mmc$ symmetry. Our calculations show a pressure-induced phase transition into this new phase from the cubic phase believed to be observed in experiment [25, 26]. The overall phase behaviour predicted within the harmonic picture is $C2/m \rightarrow Fm\bar{3}m \rightarrow P6_3/mmc$ with all three of these phases predicted to be high-T_c superconductors. Making the assumption that unstable modes can be neglected, however, gives the same picture as the anharmonic calculations of Ref. [24] where $Fm\bar{3}m$ is the true ground state at lower pressures. The new hexagonal phase predicted here offers a direct explanation for the observation of hcp impurities in recent experiments [26].

We found that YH$_{10}$ adopts very similar structures to LaH$_{10}$, with one of $P6_3/mmc$ symmetry again amongst the most energetically competitive candidates. Over the pressure range considered the $Fm\bar{3}m/R\bar{3}m$ phase remains the most stable. The difference in Gibbs free energy between these two structures is extremely small, meaning synthesis of a pure sample of either could be difficult.

We found the double-delta smearing employed in superconductivity calculations to be of particular importance. Its effect on calculated T_c changes from system to system; in particular, in our calculations the default minimum smearing employed by QUANTUM ESPRESSO overestimates T_c for LaH$_{10}$ by ∼20 K and YH$_{10}$ by ∼30 K when compared to optimal smearing.

[1] N. W. Ashcroft, Phys. Rev. Lett. **21**, 1748 (1968).
[2] J. M. McMahon, M. A. Morales, C. Pierleoni, and D. M. Ceperley, Rev. Mod. Phys **84**, 1607 (2012).
[3] H.-K. Mao and R. J. Hemley, Science **244**, 1462 (1989).
[4] M. Eremets and I. Troyan, Nature Materials **10**, 927 (2011).
[5] P. Dalladay-Simpson, R. T. Howie, and E. Gregoryanz, Nature **529**, 63 (2016).
[6] R. P. Dias and I. F. Silvera, Science **355**, 715 (2017).
[7] P. Loubeyre, F. Occelli, and P. Dumas, Nature **577**, 631 (2020).
[8] N. W. Ashcroft, Phys. Rev. Lett. **92**, 187002 (2004).
[9] D. Duan, Y. Liu, Y. Ma, Z. Shao, B. Liu, and T. Cui, Natl. Sci. Rev **4**, 121 (2017).
[10] E. Zurek and T. Bi, J. Chem. Phys. **150**, 050901 (2019).
[11] J. A. Flores-Livas, L. Boeri, A. Sanna, G. Profeta, R. Arita, and M. Eremets, Physics Reports (2020), https://doi.org/10.1016/j.physrep.2020.02.003.
[12] L. Boeri and G. B. Bachelet, J. Phys: Condens. Matt. **31**, 234002 (2019).
[13] A. R. Oganov, C. J. Pickard, Q. Zhu, and R. J. Needs, Nature Reviews Materials **4**, 331 (2019).
[14] R. J. Needs and C. J. Pickard, APL Materials **4**, 053210 (2016).
[15] C. J. Pickard, I. Errea, and M. I. Eremets, Annual Review of Condensed Matter Physics **11**, 57 (2020).
[16] A. P. Durajski and R. Szczesniak, Supercond. Sci. and Tech. **27**, 115012 (2014).
[17] D. Y. Kim, R. H. Scheicher, and R. Ahuja, Phys. Rev. Lett. **103**, 077002 (2009).
[18] Y. Li, J. Hao, H. Liu, J. S. Tse, Y. Wang, and Y. Ma, Scientific Reports **5**, 9948 (2015).
[19] C. Heil, S. di Cataldo, G. B. Bachelet, and L. Boeri, Phys. Rev. B **99**, 220502(R) (2019).
[20] H. Liu, I. I. Naumov, R. Hoffmann, N. W. Ashcroft, and R. J. Hemley, Proc. Nat. Acad. Sci. **114**, 6990 (2017).
[21] F. Peng, Y. Sun, C. J. Pickard, R. J. Needs, Q. Wu, and Y. Ma, Phys. Rev. Lett. **119**, 107001 (2017).
[22] Z. M. Geballe, H. Liu, A. K. Mishra, M. Ahart, M. Somayazulu, Y. Meng, M. Baldini, and R. J. Hemley, Angewandte Chemie International Edition **57**, 688 (2018).

[23] H. Liu, I. I. Naumov, Z. M. Geballe, M. Somayazulu, J. S. Tse, and R. J. Hemley, Phys. Rev. B **98**, 100102(R) (2018).

[24] I. Errea, F. Belli, L. Monacelli, A. Sanna, T. Koretsune, T. Tadano, R. Bianco, M. Calandra, R. Arita, F. Mauri, and J. A. Flores-Livas, Nature **578**, 66 (2020).

[25] M. Somayazulu, M. Ahart, A. K. Mishra, Z. M. Geballe, M. Baldini, Y. Meng, V. V. Struzhkin, and R. J. Hemley, Phys. Rev. Lett. **122**, 027001 (2019).

[26] A. P. Drozdov, P. P. Kong, V. S. Minkov, S. P. Besedin, M. A. Kuzovnikov, S. Mozaffari, L. Balicas, F. F. Balakirev, D. E. Graf, V. B. Prakapenka, E. Greenberg, D. A. Knyazev, M. Tkacz, and M. I. Eremets, Nature **569**, 528 (2019).

[27] N. P. Salke, M. M. D. Esfahani, Y. Zhang, I. A. Kruglov, J. Zhou, Y. Wang, E. Greenberg, V. B. Prakapenka, J. Liu, A. R. Oganov, and J.-F. Lin, Nature Communications **10**, 1 (2019).

[28] X. Li, X. Huang, D. Duan, C. J. Pickard, D. Zhou, H. Xie, Q. Zhuang, Y. Huang, Q. Zhou, B. Liu, and T. Cui, Nature Communications **10**, 3461 (2019).

[29] D. Zhou, D. V. Semenok, D. Duan, H. Xie, W. Chen, X. Huang, X. Li, B. Liu, A. R. Oganov, and T. Cui, Science Advances **6** (2020), 10.1126/sciadv.aax6849, https://advances.sciencemag.org/content/6/9/eaax6849.full.pdf.

[30] D. Zhou, D. V. Semenok, H. Xie, X. Huang, D. Duan, A. Aperis, P. M. Oppeneer, M. Galasso, A. I. Kartsev, A. G. Kvashnin, A. R. Oganov, and T. Cui, Journal of the American Chemical Society **142**, 2803 (2020).

[31] P. Hohenberg and W. Kohn, Phys. Rev **136**, B864 (1964).

[32] W. Kohn and L. J. Sham, Phys. Rev **140**, A1133 (1965).

[33] F. Giustino, Rev. Mod. Phys. **89**, 015003 (2017).

[34] P. Giannozzi, S. Baroni, N. Bonini, M. Calandra, R. Car, C. Cavazzoni, D. Ceresoli, G. L. Chiarotti, M. Cococcioni, I. Dabo, A. Dal Corso, S. de Gironcoli, S. Fabris, G. Fratesi, R. Gebauer, U. Gerstmann, C. Gougoussis, A. Kokalj, M. Lazzeri, L. Martin-Samos, N. Marzari, F. Mauri, R. Mazzarello, S. Paolini, A. Pasquarello, L. Paulatto, C. Sbraccia, S. Scandolo, G. Sclauzero, A. P. Seitsonen, A. Smogunov, P. Umari, and R. M. Wentzcovitch, Journal of Physics: Condensed Matter **21**, 395502 (19pp) (2009).

[35] P. Giannozzi, O. Andreussi, T. Brumme, O. Bunau, M. B. Nardelli, M. Calandra, R. Car, C. Cavazzoni, D. Ceresoli, M. Cococcioni, N. Colonna, I. Carnimeo, A. D. Corso, S. de Gironcoli, P. Delugas, R. A. DiStasio, A. Ferretti, A. Floris, G. Fratesi, G. Fugallo, R. Gebauer, U. Gerstmann, F. Giustino, T. Gorni, J. Jia, M. Kawamura, H.-Y. Ko, A. Kokalj, E. Küçükbenli, M. Lazzeri, M. Marsili, N. Marzari, F. Mauri, N. L. Nguyen, H.-V. Nguyen, A. O. de-la Roza, L. Paulatto, S. Poncé, D. Rocca, R. Sabatini, B. Santra, M. Schlipf, A. P. Seitsonen, A. Smogunov, I. Timrov, T. Thonhauser, P. Umari, N. Vast, X. Wu, and S. Baroni, Journal of Physics: Condensed Matter **29**, 465901 (2017).

[36] Our optimisations have been submitted to the QUANTUM ESPRESSO project.

[37] G. M. Eliashberg, Sov. Phys. JETP **11**, 696 (1960).

[38] `http://elk.sourceforge.net/`, the ELK FP-LAPW code.

[39] M. Wierzbowska, S. de Gironcoli, and P. Giannozzi, arXiv:cond-mat/0504077 (2005).

[40] J. P. Perdew, K. Burke, and M. Ernzerhof, Phys. Rev. Lett. **77**, 3865 (1996).

[41] P. Blaha, K. Schwarz, G. K. Madsen, D. Kvasnicka, and J. Luitz, `http://www.wien2k.at/reg_user/textbooks/usersguide.pdf/` (2001), wien2k user guide.

[42] See supplementary information.

[43] I. A. Troyan, D. V. Semenok, A. G. Kvashnin, A. V. Sadakov, O. A. Sobolevskiy, V. M. Pudalov, A. G. Ivanova, V. B. Prakapenka, E. Greenberg, A. G. Gavriliuk, V. V. Struzhkin, A. Bergara, I. Errea, R. Bianco, M. Calandra, F. Mauri, L. Monacelli, R. Akashi, and A. R. Oganov, arXiv preprint arXiv:1908.01534 (2020).

[44] P. P. Kong, V. S. Minkov, M. A. Kuzovnikov, S. P. Besedin, A. P. Drozdov, S. Mozaffari, L. Balicas, F. F. Balakirev, V. B. Prakapenka, E. Greenberg, D. A. Knyazev, and M. I. Eremets, arXiv preprint arXiv:1909.10482 (2019).

[45] C. J. Pickard and R. J. Needs, J. Phys: Condens. Matt. **23**, 053201 (2011).

[46] S. J. Clark, M. D. Segall, C. J. Pickard, P. J. Hasnip, M. I. J. Probert, K. Refson, and M. C. Payne, Zeitschrift für Kristallographie-Crystalline Materials **220**, 567 (2005).

[47] M. Rutter, Computer Physics Communications **225**, 174 (2018).

[48] F. Birch, Phys. Rev. **71**, 809 (1947).

[49] P. Morel and P. W. Anderson, Phys. Rev. **125**, 1263 (1962).

[50] I. A. Kruglov, D. V. Semenok, H. Song, R. L. Szczesniak, I. A. Wrona, R. Akashi, M. M. D. Esfahani, D. Duan, T. Cui, A. G. Kvashnin, and A. R. Oganov, Phys. Rev. B **101**, 024508 (2020).

[51] C. B. Barber, D. P. Dobkin, and H. T. Huhdanpaa, ACM Trans. on Mathematical Software **22**, 469 (1996).

[52] C. Heil, G. B. Bachelet, and L. Boeri, Phys. Rev. B **97**, 214510 (2018).